Analysis of Waves in Saturn's Dayside Magnetosphere: Voyager 1 Observations

By

R. P. Lepping[1], E. C. Sittler, Jr.[1], W. H. Mish[1],

S. A. Curtis[1], and B. T. Tsurutani[2]

1. NASA/Goddard Space Flight Center, Laboratory for Extraterrestrial Physics

2. Jet Propulsion Laboratory

ABSTRACT

Magnetic field fluctuations were observed in the data of Voyager 1 on its inbound leg in Saturn's magnetosphere from about 19 to 8.4 Saturn radii, during the interval 7-17 hours before closest approach. These low amplitude oscillations had the appearance of irregular micropulsations. The wave periods in the spacecraft frame varied between ≈ 1 and 20 minutes with a tendency to be inversely correlated with the field strength. An eigenfunction analysis yielding wave propagation direction as a function of frequency showed that at and near peak frequency two distinct types of waves were present, one propagating along field lines (within 30°) usually at the higher frequencies considered, (4-14) x 10^{-3} Hz, and the other propagating along $\hat{\phi}$ (the azimuthal direction in a standard spherical coordinate system) at lower frequencies, (0.8-4) x 10^{-3} Hz. The power spectral density [in $(nT)^2/Hz$] at the peaks tended to be inversely related to frequency over the full set of frequencies. An interpretation of these results is that Alfven waves are propagating along field lines at the higher frequencies with wavelengths between 1/4 and 1/2 R_S. These occur in both the mantle and plasma sheet. The waves traveling along $\hat{\phi}$ which are observed to occur in the low latitude plasma mantle, are apparently manifestations of rapidly corotating MHD waves with large compressional components and are probably due to the operation of the centrifugal flute instability at the plasma sheet-mantle boundary. For both types wave absorption occurs with a high frequency cutoff at or near the gyrofrequency of O^+ (and/or N^+). Our results establish the framework for MHD waves within Saturn's outer magnetosphere and it is expected that the Cassini Mission, which is planned to go into orbit on July 1, 2004, will add considerably to that presented here.

1.0 Introduction

In this paper we look for evidence of MHD waves in Saturn's dayside magnetosphere by using magnetic field measurements from the Voyager 1 magnetometer (Behannon, 1977; Ness et al., 1981, 1982). Because heavy ions are known to be an important constituent of Saturn's magnetospheric plasma (Frank et al., 1980; Bridge et al., 1981, 1982; Lazarus and McNutt, 1983; Richardson, 1986), in contrast to the situation at Earth where protons generally dominate the plasma composition (Gloeckler et al., 1985), any existing MHD wave modes are expected to be confined to frequencies below the ion gyrofrequency Ω_i of the heavier ions. Such heavy ions may be N^+ and/or O^+, for example, whose gyrofrequencies are considerably below that for protons, Ω_p (i.e., $\Omega_i << \Omega_p$). Evidence for such low frequency waves near the Dione L-shell using Pioneer 10 magnetometer date were presented by Smith and Tsurutani (1983), who argued for a heavy ion plasma dominated by O^{++} which was consistent with the Pioneer 10 plasma observations reported by Frank et al. (1980). Barbosa (1993) later reported the observation of ion cyclotron waves in the vicinity of Dione's L shell using the Voyager magnetometer data. It is important to look for such waves in Saturn's magnetosphere, because they can contribute to particle energization and precipitational losses of plasma within the magnetosphere with subsequent auroral emissions from Saturn. (See review article on MHD waves at earth by Southwood and Hughes, 1983). Here, we note that in order to identify certain waves as ion cyclotron waves (i.e., left-handed waves), the ambient plasma ions, within which the pickup ions are forming, must have a large pressure anisotropy $T_\perp/T_{||} >> 1$ (see, Araneda et al., 2002). As discussed in Sittler et al. (2004), they show that within Saturn's outer magnetosphere there is a hot suprathermal component where $T_\perp/T_{||} >> 1$. Therefore, our interpretation of field-aligned propagating ion cyclotron waves within Saturn's outer magnetosphere is justified. The hot ion plasma observed by the Voyager plasma instrument (Eviatar et al., 1983; Lazarus and McNutt, 1983; Richardson, 1986) could be the result of ionized neutrals being picked up within Saturn's

rotating magnetosphere. These neutrals may originate from the spatially extensive neutral clouds of Titan (Broadfoot et al., 1981; Strobel and Shemansky, 1982; Sandel et el., 1982; Eviatar and Podolak, 1983; Barbosa, 1987; Ip, 1992; Strobel et al., 1992; Lammer and Bauer, 1993; Shemantovich, 1998; Shemantovich, 1999; Shemantovich et al., 2001; Shemantovich et al., 2003; Sittler et al., 2004a), the inner Saturnian satellites, Enceladus, Tethys, Dione and Rhea (Lanzerotti et al., 1983; Johnson et al., 1989; Johnson and Sittler, 1990; Richardson et al., 1986; Richardson et al., 1998; Jurac et al., 2001a; Sittler et al., 2004b), the E-ring and main ring system (Jurac et al., 2001b; Jurac et al., 2002), the OH cloud centered on Enceladus' L shell (Shemansky et al., 1993; Richardson et al., 1998), the atomic hydrogen cloud (Shemansky and Hall, 1992) and Saturn (Broadfoot et al., 1981), and then be ionized by solar UV, magnetospheric electrons or charge exchange reactions with magnetospheric ions. Magnetospheric electron properties have been reported by Sittler et al. (1983) and Maurice et al. (1996). For heavy ions such as N^+ and/or O^+ this pickup energy can be ~ 1.8 keV at L ~ 15. Although not detected within Saturn's magnetosphere due to their low frequencies, lower hybrid waves generated from these picked up ions, which will contribute to the formation of a ring distribution in the ion distribution function, can energize electrons along the magnetic field B with energies ~1 keV (see for example Barbosa et al., 1985, 1987). This may account, in part, for the hot electron component (T_H ~ 500 eV) observed within Saturn's magnetosphere, which seems to be associated with the presence of hot ions (Sittler et al., 1983). Hydromagnetic surface waves which mode-convert to kinetic Alfvén waves can accelerate electrons along B with energies ~ 1 keV and produce Saturn kilometric radiation (Curtis et al., 1986). At energies greater than 20 keV the Low Energy Charged Particle Experiment (LECP) has provided evidence of particle energization between the L shells of Dione and Rhea (Krimigis et al., 1982), which may be caused by disturbances set up within the magnetosphere by these satellites.

Some of the particle losses observed within the magnetosphere may be caused by plasma

waves. Electron whistler-mode waves, which occur at frequencies too high to be measured by the magnetometer but can be observed by the plasma wave experiment on Voyager (see Gurnett et al., 1981; Scarf et al., 1982; Scarf et al., 1984), may account for the depletion of hot electrons at Saturn (Sittler et al., 1983). The same can be said for the precipitation of ions by MHD waves with frequencies $\Omega < \Omega_i$ which should be within the passband of the Voyager magnetometers (Behannon et al., 1977). Hence, the magnetic field data was examined for such waves.

When the Voyager 1 magnetic field, measured during the inbound pass of Saturn's magnetosphere, was displayed as a difference field (defined below), it became evident that small amplitude fluctuations in the field were generally present from just inside the magnetopause (MP) at r ~ 23 Rs (where R_S = 60,330 km) to radial distances r ≈ 8 R_S, well inside the so-called mantle region (Krimigis et al., 1981). Near the equatorial plane the mantle region lies between the plasma sheet's outer boundary at r ~ 15 R_S and the dayside MP boundary at r ~ 23 R_S. In the mantle region small scale plasma enhancements are observed (Sittler et al., 1981, 1983) which have been attributed by Eviatar et al. (1982, 1983) to plumes of Titan and by Goertz (1983) to detached plasma islands that have broken off from the outer boundary of the plasma sheet, because of a centrifugally driven flute instability. In both models it is believed that these plasma enhancements last only a few Saturn rotation periods after which they are lost down the Saturnian magnetotail as a magnetospheric wind, similar to that observed in the distant jovian tail (Sittler et al., 1987). In this same region the hot plasma at energies > 20 keV appears to be quasi-trapped (Krimigis et al., 1981). For the regions studied these variations in the field had apparent periods in the range from ~ 1 to ~ 20 min in the spacecraft frame of reference. This paper presents power spectra analyses of these fluctuations for various sample intervals along Voyager l's path in an attempt to characterize these waves.

2.0 Trajectory and Analysis Interval

Figure 1 shows the trajectory of Voyager 1 in Saturn's magnetosphere in cylindrical coordinates (z vs. $\rho = \sqrt{x^2 + y^2}$ where z is the axial coordinate and x and y lie in the equatorial plane). The path along which the analysis of the data was made is shown as a heavy line starting at 0600 U.T. and ending at 1700 U.T. on day 317 of 1980, spanning part of the spacecraft's inbound leg to closest approach (C.A.) to Saturn. The interval covers a Saturn-centered radial extent from 19 to 8.4 R_S, with corresponding latitudinal range from -1.5° to -12.6° with respect to the equatorial plane. Along this path the spacecraft encounters the mantle, i.e., the detached plasma region, over the period 0600 U.T. to about 1030 U.T. (r: 18 - 15 R_S) and traverses the extended plasma sheet region over the remainder of the time to 1700 U.T. A sketch of these regions as shown in Figure 1 is adapted from Sittler et al. (1983). The (dashed) magnetic field lines are displayed for attitude reference. The overall analysis interval covers the middle and outer magnetosphere regions of Saturn's dayside excluding a brief region around Titan. As the spacecraft crossed the MP at ≈ 1300 L.T. it was only about 16° off the planet-sun line longitudinally.

3.0 Data and Analysis

The fluctuations in the field, especially the low amplitude fluctuations nearer 8 R_S, are more easily revealed when difference fields are computed and displayed. To do this we generated fourth-order polynomial fits to the components of 9.6-s averages of the field in spherical coordinates (r, θ, ϕ) for 4-hr intervals, subtracted these fits from the individual averages and displayed only the central 3-hrs to avoid deleterious boundary effects caused by the fitting procedure. The spherical coordinate system is defined such that $\hat{r}$ is radially away from the planet's center, $\hat{\phi}$ is parallel to the equator plane and positive counterclockwise looking down from the north pole (i.e., positive in the direction of corotation), and $\hat{\theta} = \hat{\phi} \times \hat{r}$, so that $\hat{\theta}$ points southward at the equator. Figure 2 shows an example of the difference field for a 2-hr segment, 0900 to 1100 U.T., on Day 317, 1980; also the pythagorean root mean square (RMS) deviation is

shown in the bottom panel. At this time the magnitude of the field was about 6 nT. According to Lazarus and McNutt (1983) this interval corresponds to the transition region between the mantle and plasma sheet.

One of the most striking features of these data is that they appear to be similar to irregular micropulsations in the Earth's magnetosphere (Jacobs, 1970). In the top panel of Figure 2 we identify one of the analysis intervals (10 20:35 UT$\leftrightarrow$10 32:31 UT) used in the study; it happens to be the shortest interval used. Notice that in ΔB_r the waves in this interval appear to show a significant monochromatic component, and the associated RMS is slightly enhanced over most previous values. We now describe the steps taken to perform the power spectral analyses.

In practice the analyses were carried out using as "raw' data 1.92-s component averages which were further averaged to "points" with lengths of 1.92-s x n, where n varied according to what nyquist frequency (ν_{nyq}) was desired; over all intervals studied n took values from 3 to 8. Second, we detrended the data by subtracting from them local component polynomial fits of order (p) 2, 4, or 6, depending on the length and background complexity of the specific analysis interval. [We also performed the power spectra analysis without this detrending and obtained similar results as far as determining where, in frequency, the peak in power spectral density (P.S.D.) lay. The detrending accentuated the peak and slightly modified the amount of P.S.D., which was of lesser importance to us. In any case, the relative P.S.D. from event to event was more or less the same with or without the detrending.] Third, we multiplied the data by a 10% cosine window, in order to eliminate fallaciously induced power at the higher frequencies. Other types of windows were used, as well as no windowing, with less desirable results according to our subjective judgment. Fourth, we applied a Fast Fourier Transform method of determining the P.S.D. as a function of frequency $\nu = 0$ to ν_{nyq}. The power was smoothed by averaging the P.S.D. over some small number (m) of frequency buckets; m was almost always 3. The signal processing system used had the ability to determine the minimum variance direction of the waves

as a function of frequency bucket and provide us with an estimate of the wave propagation direction ($\pm\hat{k}$). The minimum variance direction (1) is accepted as the propagation direction only if it has physical relevance; we will see below that this will be the case. In general, however, the minimum variance direction is not uniquely the $\pm\hat{k}$ direction. Finally, we displayed the resulting component and magnitude spectra and the associated time series in the minimum variance coordinate system(s) for the frequencies (one or sometimes two) corresponding to the peak P.S.D. All of the above operations are described by Mish et al. (1984).

Figure 3 shows an example of the power spectrum analysis for the 12-min analysis interval pointed out in Figure 2. We display the trace of the P.S.D. matrix as a function of frequency, where ν_{nyq} = 0.087 Hz; in this case n = 3, p = 2, and m = 3. The trace is the sum of the P.S.D.'s of the three components. The spectrum is plotted on linear scales for both ordinate and abscissa. This was done to accentuate the peak. Also note that there is no power [above ~ 10^{-3} $(nT)^2$ /Hz] at zero frequency as a result of successfully detrending the data. There were 11 degrees of freedom (see discussion below), and therefore at the 90% confidence level each P.S.D. estimate has an associated error range from (P.S.D.) x 2.1 to (P.S.D.) x $(2.l)^{-1}$, for maximum to minimum limits at each estimate (see Mish et al., 1984). The peak in the spectrum is composed of power from two adjacent frequencies, ν_{p1} = 1 x ν_{nyq}/22 and ν_{p2} = 2 x ν_{nyq}/22; the P.S.D.'s for the first three estimates are denoted by large dots for emphasis. The inset, which displays $\hat{k}\bullet\hat{B}$ vs. frequency (where $\hat{B}$ is the unit vector $B/|B|$), shows that the first frequency (ν_{p1}) corresponds to waves propagating approximately perpendicular to B. It was also shown that the acute angle between $\hat{k}$ and $\hat{\phi}$ was 32° at this frequency, so the waves are propagating nearly azimuthally. By contrast the second frequency (ν_{p2}) and succeeding frequencies correspond to waves traveling nearly along magnetic field lines, but we do not know the sense of the propagation. Note that at the highest frequencies $\hat{k}\bullet\hat{B}$ is meaningless, because of the associated low power. We consider the P.S.D.'s for points 3 and higher not to be significant. It is interesting that the gyrofrequency

for O^+ (0.0099 Hz for B = 10.0 nT) lies between the second and third frequencies where a precipitous drop in power occurs. [Note that $\nu_g(N^+)$ at B = 10.0 nT is 0.011 Hz, so it also occurs near the sharp drop in power.] As we will see later, this feature was typical of most of the computed spectra. The position of the gyrofrequency for protons lies far to right in this figure, and off the plot.

We chose eight different analysis intervals over the range $8.5 < R < 17\ R_S$ to be power-spectral analyzed according to the procedure outlined above. Table 1 lists those intervals, the specific parameters (n,p,m) used, and the results; most quantities are defined in the footnotes to the Table. Degrees of freedom (d.o.f.), footnote 9, are calculated from

$$\text{d.o.f.} = 2\ N/M \qquad (1)$$

where M is the number of frequency buckets across the spectrum after averaging over m raw P.S.D.-estimates per final bucket, and where $N = \Delta t/(1.92xn)$, Δt is the analysis interval length in seconds, and n is the number of 1.92-s points in the averages in the time-series used in the analysis (see Mish et al., 1984). The ratio ($\Delta B/B$), footnote 8, is estimated indirectly in the following way. We assume that $(\Delta B)^2 \approx [(\text{P.S.D.})_p \times (2\nu)_p/2]$, where the subscript p refers to peak values, the factor of 2 in the numerator accounts for the fact that in most cases the "peak" is $2\nu_p$ wide at the base and is symmetrical, and the 2 in the denominator accounts for the spectrum's approximate triangular shape; all power at frequencies higher than at the rapid drop at $\approx 2\nu_p$ is assumed to be zero. We also assume that $B \approx \langle B \rangle$ as given in Table 1. Hence, where P_p is the P.S.D. at the peak. Notice that all ($\Delta B/B$) listed in the table are much smaller than unity.

We point out that, even though only 8 analysis-intervals were examined, Table 1 provides P.S.D. estimates for 14 frequency buckets due to the fact that most of the spectra provided significant power for more than one bucket, as the example in Figure 3 demonstrated. Also note that the P.S.D.'s listed in the Table are those associated with the B-field component in the

maximum variation plane, i.e., that with the highest power. This was determined after the spectra were displayed in the variance coordinate system. How well the minimum variance direction was estimated is determined by the eigenvalue ratios at a given frequency. Those are listed in columns 9 and 10 of the Table where E_1, E_2, and E_3 are the eigenvalues for the maximum, intermediate, and minimum variance directions, respectively. The ideal situation for finding a well-determined propagation direction, $\hat{k}$, presumably the minimum variance direction, is when the variance ellipsoid is pancake in shape, not cigar shaped. For a good pancake the ratio E_2/E_3 should be large, at least ~ 4, and the ratio E_1/E_2 should not be too large, i.e., it should be under 10. Notice that these ratios satisfy these criteria in almost all (≈ 80%) cases displayed in Table 1. The next section discusses various important characteristics of these waves as revealed in the Table.

4.0 Wave Properties

The bottom of Figure 4 shows a plot of P.S.D. vs. frequency at the peaks of the events listed in Table 1 and labeled according to analysis interval length, shown by the key in the box. First, we see that there is a tendency for the P.S.D. to decrease with increasing frequency, and this tendency is related, at least weakly, to the propagation direction as shown in the top panel. There we plot the angle between $\hat{k}$ and $\hat{B}$ [$\angle(\hat{k},\hat{B})$] also as a function of frequency. Just as in the example in Figure 3 the waves fall into two types: type 1 will refer to those waves where $\angle(\hat{k},\hat{B}) \geq 66°$ and type 2 are those where $\angle(\hat{k},\hat{B}) \leq 30°$. It also turns out that type 1 waves propagate (i.e., the $\pm\hat{k}$ direction) along $\hat{\phi}$, the magnetosphere's corotation direction, within 35° with only one exception where $\angle(\hat{k},\hat{B})$ was 59°. All of the frequencies shown here are determined in the spacecraft frame of reference, and it is wel1 known that the magnetospheric plasma is rotating rapidly with a speed that depends on r. However, for the type 2 waves which propagate along $\hat{B}$, the estimated frequency in the spacecraft frame of reference is very close to

that in the plasma frame due to the fact that $\hat{B} \perp \hat{\phi}$ within a few degrees. But the doppler shift in frequency for type 1 waves is considerable, since they propagate along the corotation direction, or opposite it. One might question whether the type 1 "waves" are waves at all, but rather the signature of spatial (and temporal) variations of the B-field as it is convected past the spacecraft. We believe that the signature observed is a result of a combination of propagation and convection as discussed in the next section.

Figure 5 shows the average B-field vs. peak frequency, ν_p, (and period, at the top) for the events of Table 1. For comparison the gyrofrequencies of O^+ and H^+ are also shown. The gyrofrequency for N^+ would be almost the same as that for O^+. The dashed line represents an average of the two least-squares fits, where <B> and ν_p exchange roles as independent variable, to all of the points whose ordinate values are less than <B> = 27 nT. The correlation coefficient for each fit was 0.498, and the RMS $\{\nu_p\}$ was 2.51 x 10^{-3} Hz. Notice that the solid line for ν_g (O^+) and the dashed line are nearly parallel with an average offset between them of only $\Delta\nu = \nu_g(O^+) - \nu_p \approx 4x10^{-3} Hz$. So with only three exceptions (where <B> < 27 nT) the events had peak frequencies that on average were only 0.004 Hz away from the local O^+ (or N^+) gyrofrequency, just as the example in Figure 3 indicated for the type 2 waves. In all of these events the P.S.D. was significantly lower at frequencies beyond ~ $3\nu_p$ (and often beyond ~ $2\nu_p$) than at the peak. This behavior is a strong indication that the O^+ (or N^+) ion is absorbing wave energy at its (or their) gyrofrequency (if both ions are present) and therefore ν_g(O+) is a cutoff frequency for the lower frequency waves. This appears to hold for both type 1 and type 2 waves, but the case for type 1 is weaker; type 1 cluster at the far left in the figure. This will be discussed below.

We now wish to examine the question of whether or not there is a preference for a particular region with respect to wave type and power. Figure 6 shows P.S.D. (again at the peak) vs. distance from Saturn (r) and vs. planetographic latitude (LAT), with wave type distinguished

according to the key in the box to the right. The vertical dashed line denotes the approximate boundary between the plasma sheet and mantle regions for the Voyager 1 encounter (Sittler et al., 1983 and Lazarus and McNutt, 1983). The "point" represented by a solid square at 8.4 R_S is the exceptional case (code 13 in Table 1) where $\angle(\hat{k},\hat{\phi}) = 59°$ and therefore within our ability to distinguish, is neither a type 1 or 2 wave. Probably the most salient feature in the figure is the tendency for the P.S.D. at the peaks to decrease with decreasing r. Almost equally striking is the exclusivity of type 2 waves in the plasma sheet region and the predominance (but not exclusivity) of type 1 waves in the mantle. Hence, the higher frequency [ν_p: ($4 \leftrightarrow 14$ x10^{-3} Hz], lower power waves which propagate along B-field lines (within 30°) tend to prefer the plasma sheet region, and the lower frequency [ν_p: ($0.8 \leftrightarrow 4$) x 10^{-3} Hz], higher power "waves" which propagate/convect along the $\hat{\phi}$ direction (also within 30°) tend to prefer the mantle region. We stress, however, that the type 2 waves occur in both regions. It should be pointed out (and more on this in the next section) that the spacecraft was in or very near the equatorial plane when in the mantle region but was at higher latitudes while in the plasma sheet, as shown by LAT at the bottom of the figure.

Finally we call attention to the type 1 waves seen at about 8.7 R_S in the figure which seems out of place in a world of type 2 waves. As pointed out, the hybrid case, denoted by the square, also occurs near here (8.4 R_S). It is conceivable that the presence of Rhea at 8.73 R_S is producing these signatures, but it is more likely that (without more extensive analysis) the particular location of these features is coincidental.

Summary and Discussion

The observational and analytical findings of this study are:

1. Irregular low amplitude fluctuations in the magnetic field were observed along the Voyager 1 inbound leg to Saturn in the dayside magnetosphere: 19 $\leftrightarrow$ 8.4 R_S (mantle and plasma sheet regions).
2. P.S.D. $[(nT)^2/Hz]$ at peaks in spectra tends to be inversely related to frequency.
3. Propagation directions:

   Type 1: Approximately along $\pm\hat{\phi}$ for ν_p: (0.8 $\leftrightarrow$ 4) x 10^{-3} Hz, and they are also convected.

   Type 2: Approximately along $\pm\hat{B}$ for ν_p: (4 $\leftrightarrow$ 14) x 10^{-3} Hz; doppler shift is negligible.
4. Type 1 occur in mantle (near equator).

   Type 2 occur in both regions, predominantly in plasma sheet (and observed off equator).
5. Both types have a sharp drop in P.S.D. at or near the gyrofrequencies of O^+, N^+, and it remains low beyond those frequencies; this cutoff is well determined for type 2 and less so for type 1.

We now consider the nature of these fluctuations starting with type 2. The fact that these have the general appearance of irregular micropulsations in the B-field time series (see Figure 2, for example), and considering the particular frequency range covered, suggests that they are probably MHD waves. Because of their direction of propagation ($\approx$ along $\pm\hat{B}$) , we will assume that they are Alfven waves. (Note that for frequencies of these waves near the O^+/N^+ ion gyrofrequency it is more appropriate to use the term ion cyclotron waves in describing them, but at lower frequencies the term Alfvén waves is more appropriate. For simplicity of discussion below we use "Alfvén waves" in all cases.)

In order to estimate the wavelengths, λ, typical of the type 2 (Alfven) waves in the plasma sheet,

we simply assume that

$$\lambda \approx V_A \tau_p \tag{3}$$

where

$$V_A = \langle B \rangle (4\pi\rho)^{-1/2} \tag{4}$$

and τ_p is the wave period at the peak of the spectrum. We further assume that the density consists principally of contributions from thermal protons and O^+ in the density-ratio characteristic of the region of interest as suggested by Lazarus and McNutt (1983): $n_{O+}/n_p \approx 4$. The total ion mass density then is

$$\rho = \rho_p + \rho_{O+} = m_p (n_p + 16 n_{O+}),$$

or

$$\rho \approx 13 m_p n_e, \tag{5}$$

where $n_e = n_p + n_{O+}$, m_p is the proton mass, and n_e, n_p, and n_{O+} are the electron, proton, and O^+ number densities, respectively. We consider an average of n_e of 0.75 cm^3 as being typical for the plasma sheet over the Voyager 1 path of interest, where $0.5 < n_e < 1.0$ cm^{-3}; see Sittler et al. (1983). Hence, $V_A \approx 7.0$ B km/s, where B is in nT. (It can be shown that V_A is only very weakly dependent on the value chosen for n_{O+}/n_p). We now examine two extreme cases, i.e., (1) at R = 8.5 R_5 where B is largest (30.8 nT) and τ_p is smallest (1.2 min) and (2) at R = 13.0 R_S where B is smallest (10.4 nT) and τ_p is largest (5.6 min), within the plasma sheet. These yield

At R = 8.5 R_S, $V_A \approx 220$ km/s

and $\lambda \approx 0.26$ R_S.

At R = 13.0 R_S, $V_A \approx 73$ km/s

and $\lambda \approx 0.41\ R_S$.

Since the wavelengths of these Alfven waves are short compared to the dimension of the dayside magnetosphere, which is typically 20 R_S for the subsolar planet-to-magnetopause distance, they are not likely to be standing waves. Again we point out that the doppler shift in frequency for these waves is negligible, since they are propagating approximately along field lines which are close to being perpendicular to the direction of motion of the rotating magnetospheric plasma. The situation is quite different for the type 1 waves which we discuss below.

We now examine the scale lengths (in a plane parallel to the equator) of the type 1 plasma features seen in the mantle and believed to be rapidly convected MHD waves, where it will be assumed that the wave speed is negligible compared to the rotation speed. Hence, the length (d_ϕ) of such a feature (detached plasma island, or semidetached plasma peninsula as pictured by Goertz (1983)) along $\hat{\phi}$ is estimated by

$$d_\phi \approx V_{coro}\ \tau_p\ , \qquad (6)$$

where V_{coro} is taken to be ≈ 150 km/s in the mantle at r ≈ 16 R_S. Our estimates of τ_p in this region range from 4.2 min to 20.0 min (codes 5 and 4, respectively, in Table 1). Hence, we obtain values of 0.63 R_S to 3.0 R_S for d_ϕ, which are consistent with those estimated from the Voyager plasma data (Sittler et al., 1983). It is not easy to interpret these numbers, since the inclination (α) of these plasma elements with respect to $\hat{\phi}$ is not accurately known. But they probably represent features of much larger tangential dimensions (i.e., along $\hat{\phi}$) than the wavelengths (λ_A) of the field aligned propagating Alfven waves. Even the width (D) of these (apparently) elongated plasma blobs, in most cases, is estimated to be greater than the λ_A's, if it is assumed that D can be appropriately estimated by $D \sim d_\phi \sin\alpha$, where relative radial motions are neglected. By these we mean radial motions of the magnetospheric plasma or the spacecraft. Then D ~ ½ ↔ 2 R_S for $\alpha \sim 45°$ and d_ϕ = 0.63 ↔ 3.0 R_S. [We justify ignoring the spacecraft speed (V_S) by showing that for V_S (radial) of 17 km/s radial thicknesses are only 0.071 to 0.34 R_S for τ_p of 4.2 to 20.0 min.]

In support of our assumption that these are MHD waves traveling approximately perpendicular to field lines in the mantle, we show Figure 7, which reveals a correlation between electron density and field magnitude and various components, especially ΔB_θ which dominates ΔB. Hence, these convected MHD waves have a strong compressional component.

We interpret these findings in terms of the following:

1. The type 1 fluctuations are the convected MHD wave signatures of plasma sheet detachment into the mantle, near the equator, by the operation of the centrifugal flute instability (see Goertz, 1983, and Curtis et al . , 1986) . These waves have a strong compressional component and are rapidly convected by corotation along $\hat{\phi}$.

2. The type 2 fluctuations are Alfven waves driven by field line perturbations caused either by the type 1 fluctuations operating at the equator or by general magnetospheric plasma motions normal to $\hat{B}$. The associated Alfven speeds range from 220 km/s at 8 R_S to 70 km/s at 13 R_S, with corresponding wavelengths from 1/4 to 1/2 R_S, respectively.

3. For both types, wave absorption occurs with a high frequency cutoff at or near the gyrofrequencies of either (or both) O^+ or N^+; the cutoff is better determined for type 2.

4. The width of the "detached" plasma blobs in the mantle is roughly estimated to be ~ ½ ↔ 2 R_S.

Although the magnetic field data intervals used in this study were discriminately chosen, we believe they generally represent the state and character of the extended plasma sheet and mantle

of Saturn 's dayside magnetosphere during the passage of Voyager 1.

Concerning item 3 it may seem surprising that both wave types suffer absorption with high frequency cutoffs at the gyrofrequencies of O^+ and/or N^+, since type 1 are severely doppler shifted but type 2, to a good approximation, are not frequency-shifted. It is apparent that the type 2 waves are properly described by the frequencies as measured by the spacecraft, and therefore the O^+ cutoff-frequency has direct meaning. But the type 1 features are mainly convected structures primarily seen in the mantle, and in their case the "high-frequency-cutoff" represents a spatial scale-length cutoff, i.e., minimum size structures. Before attempting to provide physical meaning to this, we point out that the intervals that yielded $\hat{k} \parallel \hat{\phi}$ (type 1) cluster mainly in the lower left corner of Figure 5, so that their relationship to $\nu_g(O^+)$ is less certain than the type 2 cases; i.e., their relative differences $[\nu - \nu_g(O^+)]$ are usually greater. Hence, the "high-frequency-cutoff" for type 1 is not as well determined as that for type 2. From Lazarus and McNutt (1983) and Richardson (1986) we see that a typical O^+ temperature at $\approx 17\ R_S$ in the mantle is ≈ 100 eV, which converts to a thermal speed of ≈ 34 km/s. For B = 7 nT the local O^+ gyroradius for a 90° pitch angle then is $r_g(O^+) = 0.013\ R_S$. Since the shortest scale-length features in the mantle were estimated above to be $D_{min} \sim 0.5\ R_S$ we see that

$$D_{min}/r_g(O^+) \approx 40.$$

We note that the cutoff (D_{min}) being above the ion gyroradius is expected, since the waves associated with the centrifugal flute instability will have greater growth rates with increasing $k = 2\pi/\lambda$ (decreasing wavelengths) until damped in the vicinity of the ion gyroradius. Quantitatively the cutoff occurs at somewhat lower k than one would expect. However the actual growth of waves at large k may be more restricted than one would ascertain from the examination of linear temporal growth rates alone, which predicts $D_{min}/r_g(O^+) \geq .1$. In particular, the convective growth rates determined from the ratio of the growth rate to the wave's group velocity may enter to restrict the domain of higher amplitude waves to lower k, if the group velocity increases with k. Then spatial limits to amplification becomes important. This is a question that deserves further study.

Finally, it seems appropriate to compare our type 2 (Alfvén) waves with waves in Saturn's magnetosphere studied by Smith and Tsurutani (1983) and Barbosa (1993) who interpreted them to be of the ion cyclotron mode, both of which however were shown to be propagating along magnetic field lines. Focusing our attention to the Smith and Tsurutani (1983) results, it is not surprising that the characterization of the waves discussed in this paper is different from their interpretation, because we argue that they are probably observing a different type of wave. The reasons for this belief are the following. Their waves appear to be very regular and monochromatic reminding us of regular geomagnetic micropulsations (see their Figure 2), whereas ours are very irregular in appearance. Their observations were made at a smaller L, that of Dione, ≈ 6.3, than our range of about L = 8.5 to 19. Since $\Delta B \approx 5$ nT for their waves, then $\Delta B/B \approx 0.05$ at L = 6.5; our $\Delta B/B$ is approximately 0.011 on average, five times smaller. It may be, however, that both kinds of waves are associated with the same heavy ions, O^+ or N^+, directly associated with the generation of ion cyclotron waves (Smith and Tsurutani, 1983) and indirectly via Alfvén wave absorption at a high frequency cutoff in our case. Their larger $\Delta B/B$ may be due to their close proximity to Dione's orbit, whereas the source of our Alfvén waves is very likely more diffuse, especially if the waves are due to excitation from the type 1 fluctuations in the mantle or due to external changes, as we previously suggested. However, we point out that when the ~ 18-s wave periods (at $r = 6.3\ R_S$ where $\langle B \rangle \approx 72$ nT) of Smith and Tsurutani are scaled in terms of the observed magnetic field, they compare relatively well with the type 2 periods reported here. See for example, the last line in Table 1 where $r = 8.5\ R_S$ (closest to $r \approx 6.3\ R_S$) and $\tau = 1.2$ min at $\langle B \rangle = 31$ nT, showing an agreement within a factor of ≈ 1.7 with the Smith and Tsurutani's results. Hence, it may be that what Smith and Tsurutani were seeing was a disturbance in the magnetosphere set up by Dione with absorption at the ion gyrofrequency preventing the cascading of power from lower frequencies to higher frequencies.

Finally, our results were compiled in preparation for the Cassini Mission, for which orbit

insertion is planned to occur on July 1, 2004. It is expected that the Cassini Mission, with its four year tour and possible two more years of an extended mission, will add considerably to the Voyager results reported here. Our result do lay the foundation for low frequency MHD waves within Saturn's outer magnetosphere and provides direction for more comprehensive studies expected to be done by Cassini.

References:

Araneda, J. A., A. F. Vinas and H. F. Astudillo, Proton core temperature effects on the relative drift and anisotropy evolution of the ion beam instability in the fast solar wind, *J. Geophys. Res.*, **107**, doi:10.1029/2002JA009337, 2002.

Barbosa, D. D., F. V. Coroniti, W. S Kurth and F. L. Scarf, Voyager observations of lower hybrid noise in the lower hybrid noise in the Io plasma torus and anomalous plasma heating rates, *Astrophys. J.*, **289**, 392, 1985.

Barbosa, D. D., Titan's atomic nitrogen torus: Inferred properties and consequences for the Saturnian aurora, *Icarus*, **72**, 53, 1987.

Barbosa, D. D., Theory and observations of electromagnetic ion cyclotron waves in Saturn's inner magnetosphere, *J. Geophys. Res.*, **98**, 9345, 1993.

Behannon, K. N, M. H. Acuna, L. F. Burlaga, R. P. Lepping, N. F. Ness, and F. M. Neubauer, Magnetic field experiment for Voyagers 1 and 2, *Space Sci. Rev.,***21**, 235, 1977.

Bridge, H. S., 3. W. Belcher, A. J. Lazrus, S. Olbert, J. D. Sullivan, F. Bagenel, P. R. Gazis, R. E. Hartle, K. W. Ogilvie, J. D. Scudder, E. C. Sittler, Jr., A. Eviator, G. L. Siscoe, C. K. Goertz, and V. M. Vasyliunas, Plasma observations near Saturn: Initial results from Voyager 1, *Science*, **212**, 217, 1981.

Bridge, H. S., F. Bagenal, J. W. Belcher, A. J. Lazarus, R. L. McNutt, J. ID. Sullivan, P. R. Gazis, R. E. Hartle, K. W. Ogilvie, J. D. Scudder, E. C. Sittler, A. F.viatar, G. L. Siscoe, C. K. Goertz, and V. M. Vasyliunas, Plasma Observations near Saturn: Initial results from

Voyager 2, *Science*, **215**, 563, 1982.

Broadfoot , A. L. , B. R. Sandel , ID. E. Shemansky, J. B. Holberg, G, R. Smith, D. F. Strobel, J. C. McConnell, S. Kumar, D. M. Hunten, S. K. Atreya, T. M. Donahue, H. N. Moos, J. L. Bertaux, J. E. Blamont, R. B. Pomphrey, and S. Linick, Extreme ultraviolet observations from Voyager 1 encounter with Saturn, *Science*, **212**, 206, 1981.

Curtis, S. A., R. P. Lepping, and E. C. Sittler, Jr., The centrifugal flute instability and the generation of Saturn kilometric radiation, *J.Geophys. Res.*, **91**, 10,989-10,994,1986.

Eviatar A., G. L. Siscoe, J. D. Scudder, E. C. Sittler, Jr., and J. D. Sullivan, The plumes of Titan, *J. Geophys. Res.*, **87**, 8091, 1982.

Eviatar, A., R. L. McNutt, Jr., C. L. Siscoe, and J. ID. Sullivan, Heavy ions in the outer Kronian magnetosphere, *J. Geophys. Res*., **88**, 823, 1983.

Eviatar, A. and M. Podolak, Titan's gas and plasma torus, *J. Geophys. Res.*, **88**, 833-840, 1983.

Frank, L. A., B. G. Burek, K. L. Ackerson, J.H. Wolfe, and J. D. Mihalov, Plasmas in Saturn's magnetosphere, *J.Geophys. Res.*, **85**, 5695, 1980.

Gloeckler, G., B. Nilken, N. Stüdemann, F. M. Ipavich, D. Hovestadt, D. C. Hamilton, and G. Kremser, First composition measurements of the bulk of the storm-time ring current (1 to 300 keV/e) with AMPTE-CCE, *Geophys. Res. Lett.*, **12**, 325, 1985.

Goertz, C. K., Detached plasma in Saturn's front side magnetosphere, *Geophys. Res. Lett.*, **10**,

455, 1983.

Gurnett, D. A., N. S. Kurth, and F. L. Scarf, Plasma waves near Saturn: Initial results from Voyager 1, *Science*, 212, 235, 1981.

Ip, W.–H., The nitrogen tori of Titan and Triton, *Adv. Space Res.*, **12**, (8)73, 1992.

Jacobs, J. A., Geomagnetic Micropulsations, Springer-Verlag, Berlin, 1970.

Johnson, R. E., M. K. Pospicszalska, E. C. Sittler, Jr., A. F. Cheng, L. J. Lanzerotti, and E. M. Sievka, The neutral cloud and heavy ion inner torus at Saturn, *Icarus*, **77**, 311, 1989.

Johnson, R. E. and E. C. Sittler, Jr., Sputter-produced plasma as a measure of satellite surface composition: The Cassini mission, *Geophys. Res. Lett.*, **17**, 1629, 1990.

Jurac, S., R. E. Johnson, J. D. Richardson,, and C. Paranicas, Satellite sputtering in Saturn's magnetosphere, *Planet. Space Sci.*, **49**, 319, 2001a.

Jurac, S., R. E. Johnson and J. D. Richardson, Saturn's E ring and production of the neutral torus, *Icarus*, **149**, 384, 2001b.

Jurac, S., M. A. McGrath, R. E. Johnson, J. D. Richardson, V. M. Vasyliunas, and A. Eviatar, Saturn: Search for a missing water source, *Geophys. Res. Lett.*, **29(24)**, 2172, doi:10.1029/2002GL015855, 2002.

Krimigis, S. M., T. P. Armstrong, N. I. Axford, C. O. Bostrom, G. Gloeckler, E. P. Keath, L. J. Lanzerotti, J. F. Carbary, D. C. Hamilton, and E. C. Roelof, Low-energy charged particles

in Saturn's magnetosphere: Results from Voyager 1, *Science*, **212**, 225, 1981.

Krimigis, S. M., T. P. Armstrong, N. I. Axford, C. O. Bostrom, G. Gloeckler, E. P. Keath, L. J. Lanzerotti, J. F. Carbary, D. C. Hamilton, and E. C. Roelof, Low-energy hot plasma and particles in Saturn's magnetosphere, *Science*, **215**, 571, 1982.

Lammer, H. and S. J. Bauer, Atmospheric mass loss from Titan by sputtering, *Planet. Space Sci.*, **41**, 657, 1993.

Lanzerotti, L. J., C. G. Maclennan, N. L. Brown, R. E. Johnson, L. A. Barton, C. T. Reimann, J. W. Garrett, and J. W. Boring, Implications of Voyager data for energetic ion erosion of the icy satellites of Saturn, *J. Geophys. Res*., **88**, 8765, 1983.

Lazarus, A. J., and R. L. McNutt, Jr., Low-energy plasma ion observations in Saturn's magnetosphere, *J. Geophys. Res.*, **88,** 8831, 1983.

Maurice, S., E. C. Sittler, Jr., J. F. Cooper, B. H. Mauk, M. Blanc and R. S. Selesnick, Comprehensive analysis of electron observations at Saturn: Voyager 1 and 2, *J. Geophys. Res.*, **101**, 15,211 – 15,232, 1996.

Mikhailosksii, A. B., Theory of Plasma Instabilities, Vol. 2, Consultants Bureau, New York, 1974.

Mish, N. H., R. M. Wenger, K. N. Behannon, and J. B. Byrnes, Interactive digital signal processor, NASA TM-83997, revised May 1984.

Ness, N. F., M. H. Acuna, R. P. Lepping, J. E. P. Connerney, K. W. Behannon, L. F. Burlaga, and F. M. Neubauer, Magnetic field studies by Voyager 1, Preliminary results at Saturn, *Science*, **212**, 211, 1981.

Ness, N. F., M. H. Acuna, K. N. Behannon, L. F. Burlaga, J. E. P. Connerney, R. P. Lepping, and F. M. Neubauer, Magnetic field studies by Voyager 2: Prelimnary results at Saturn, *Science*, **215**, 558, 1982.

Richardson, J. D., A. Eviatar and G. L. Siscoe, Satellite tori at Saturn, *J. Geophys. Res.*, **91**, 8749, 1986.

Richardson, J. D., A. Eviatar, M. A. McGrath and V. M. Vasyliunas, OH in Saturn's magnetosphere: Observations and implications, *J. Geophys. Res.*, **103**, 20245, 1998.

Sandel , B. R., D. E. Shetnansky, A. L. Broadfoot, J. B. Hoiberg, G. R. Smith, J. C. McConwell, D. F. Strobel, S. K. Atreya, T. M. Donahue, H. N. Moos, D. M. Hunten, R. B. Pomphrey, and S. Linick, Extreme ultraviolet observations from the Voyager 2 encounter with Saturn, *Science*, **215**,548, 1982.

Scarf, F. L., D. A. Gurnett, W. S. Kurth, and R. L. Poynter, Voyage 2 plasma wave observations at Saturn, *Science*, **215**, 587, 1982.

Scarf, F. L., L. A. Frank, D. A. Gurnett, L. J. Lanzerotti, A. Lazarus and E. C. Sittler, Jr., Measurements of plasma, plasma waves and suprathermal charged particles, *Saturn*, T. Gehrels and M. S. Matthews editors, The University of Arizona Press, Tucson, Arizona, 318, 1984.

Shemansky, D. E. and D. T. Hall, The distribution of atomic hydrogen in the magnetosphere of Saturn, *J. Geophys. Res.*, **97**, 4143-4161, 1992.

Shemansky, D. E., P. Matherson, D. T. Hall, H.-Y. Hu and T. M. Tripp, Detection of the hydroxyl radical in the Saturn magnetosphere, *Nature*, **363**, 329-332, 1993.

Shemantovich, V. I., Kinetic modeling of suprathermal nitrogen atoms in the Titan's atmosphere: I. Sources, *Solar System Research*, **32**, 384, 1998.

Shemantovich, V. I., Kinetic modeling of suprathermal nitrogen atoms in the Titan's atmosphere: II. Escape flux due to dissociation processes, *Solar System Research*, **33**, 32, 1999.

Shemantovich, V. I., C. Tully and R. E. Johnson, Suprathermal nitrogen atoms and molecules in Titan's corona, *Adv. Space Res.*, **27**, 1875-1880, 2001.

Shemantovich, V. I., R. E. Johnson, M. Michael and J. G. Luhmann, Nitrogen loss from Titan, manuscript in preparation, 2003.

Sittler, E. C., Jr., J. D. Scudder, and H. S. Bridge, Detection of the distribution of neutral gas and dust in the vicinity of Saturn, *Nature*, **292**, 711, 1981.

Sittler, E. C., Jr., K. W. Ogilvie, and J. D. Scudder, Survey of low-energy plasma electrons in Saturn's magnetosphere: Voyagers 1 and 2 , *J. Geophys. Res* . , **88**, 8847, 1983.

Sittler, E. C., Jr., R. E. Johnson, S. Jurac, J. D. Richardson, M. McGrath, F. Crary, D. T. Young and J. E. Nordholt, Pickup ions at Dione and Enceladus: Cassini Plasma Spectrometer

simulations, *J. Geophys. Res.*, **109**, A01214, doi:10.1029/2002JA009647, 2004.

Sittler, E. C., Jr., R. E. Johnson, H. T. Smith, J. D. Richardson, S. Jurac, M. Moore, J. F. Cooper, B. H. Mauk, M. Michael, C. Paranicas, T. P. Armstrong and B. T. Tsurutani, Energetic nitrogen ions within the inner magnetosphere of Saturn, *J. Geophys. Res.*, submitted, 2004.

Smith, E. J., and B. T. Tsurutani, Saturn's magnetosphere: Observations of ion cyclotron waves near the Dione L Shell, *J. Geophys. Res.*, **88**, 7831, 1983.

Southwood, D. J., and W. J. Hughes, Theory of hydromagnetic waves in the magnetosphere, *Space Sci. Rev.*, **35**, 301, 1983.

Table 1

Power Spectral Parameter Values

Code No.	Time Period (U.T.)	R (R_S)	<B> (nT)	ν_g (O^+) (10^{-3}Hz)	n[1] p[2] m[3]	ν_{nyq} (10^{-3}Hz)	M[4] K[5]	E_2/E_3	E_1/E_2	ν_p[6] (10^{-3} Hz)	τ_p[7] (min)	∠(k,θ)	∠(k,ϕ)	P. S. D. $((nT)^2/Hz)$	$(\Delta B/B)^8$	d.o.f.[9]
1_	0805:23 - 0841:00	16.9	6.0	5.94	8 2 3	32.6	24 1	36.7	4.3	1.36	12.3	66.2°	31.0°	148.0	0.075	12
2	0805:23 - 0841:00	16.9	6.0	5.94	4 4 3	65.1	47 2	3.7	2.7	2.77	6.0	80.3°	14.0°	59.4	0.068	12
3	0805:23 - 0841:00	16.9	6.0	5.94	4 4 3	65.1	47 5	13.0	3.0	6.93	2.4	11.5°		2.1	0.020	12
4*	0900:35 - 1100:00	16.6 -14.6	9.3	9.20	7 6 3	37.2	90 2	4.0	1.5	0.83	20.0	86.2°	21.2°	98.1	0.031	12
5	1020:35 - 1032:31	15.1	10.0	9.90	3 2 3	86.8	22 1	3.9	2.4	3.94	4.2	76.3°	31.7°	19.3	0.027	11
6	1020:35 - 1032:31	15.1	10.0	9.90	3 2 3	86.8	22 2	2.9	4.9	7.89	2.1	20.1°		20.6	0.040	11
7	1218:11 -1251:00	13.0	10.4	10.30	6 4 3	43.4	29 2	11.2	5.6	2.99	5.6	8.9°		7.7	0.015	12
8	1218:11 - 1251:00	13.0	10.4	10.30	6 4 3	43.4	29 4	3.4	2.1	5.99	2.8	13.8°		2.8	0.012	12
9*	1300:35 - 1400:00	12.5 - 11.5	11.8	11.70	6 4 5	43.4	32 3	4.7	2.6	4.07	4.1	12.3°		36.4	0.033	19
10	1400:35 -1427:00	11.3	13.4	13.30	6 4 3	43.4	24 4	10.4	4.1	7.23	2.3	29.0°		2.1	0.009	11
11	1400:35 - 1427:00	11.3	13.4	13.30	6 4 3	43.4	24 5	13.1	1.7	9.04	1.8	7.2°		2.1	0.010	11
12*	1615:47 -1705:00	9.2 -8.4	28.0	27.70	5 4 3	52.1	52.4	8.9	2.4	4.01	4.1	86.1°	35.5°	5.9	0.005	12
13	1640:35 -1705:00	8.5	30.8	30.50	5 4 3	52.1	26 *2*	13.3	2.3	4.01	4.1	68.5°	58.6°	5.2	0.005	12
14	1640:35 - 1705: 00	8.5	30.8	30.50	5 4 3	52.1	26 7	9.9	1.2	14.03	1.2	12.1°		0.62	0.003	12

[1]n = no. of 'points' in average, [2]p = order of detrending po1ynomial, [3]m = no. of frequency buckets in average, [4]M = no. of frequency buckets across spectrum after averaging, [5]k-th frequency bucket at peak, [6]ν_p = peak frequency, [7]$\tau_p = 1/\nu_p$, [8]estimated $\Delta B/B$ (see text), and [9]d.o.f. degrees of freedom.
*Long analysis intervals, i.e. ≥ 1 hr.

Figure Captions:

Fig.1.The trajectory of Voyager 1 in Saturn's magnetosphere in cylindrical coordinates (ρ vs. z) where the z-axis is coincident with Saturn's spin axis; R_S = 60,330 km. During the inbound leg of interest, the darkened line, the spacecraft was confined to a local time of ~ 0130 L.T. longitudinally. The sketch depicting the locations of the extended plasma sheet and mantle regions are adapted from Sittler et al. (1983).

Fig.2. Example of magnetic field fluctuations occurring over a 2-hr period near the plasma sheet-mantle boundary. These difference fields are presented in spherical coordinates and were derived by subtracting a 4-th order polynomial fit of the B components from 9.6-s averages (see text).

Fig.3. The trace of the power spectral density (P.S. D.) matrix vs. frequency for the analysis interval shown in Figure 2 plotted in linear space. The inset shows the propagation direction of the waves with respect to the B-field direction vs. frequency. The propagation directions were determined from an eigenvalue analysis.

Fig.4. Lower panel: Power spectral density vs. peak frequency for eight analysis intervals (and for 14 frequency estimates) where the interval lengths are coded and shown in the box. The small dots include the short analysis interval (12 min) presented in Figure 3. Upper panel: The angle between $\hat{k}$ and $\hat{B}$ vs. peak frequency shown according to interval length. Also shown in the top portion is the acute angle between $\hat{k}$ and the corotation direction $\hat{\phi}$. The region where 0° < $\angle(\hat{k},\hat{B})$ < 30° contains type 2 waves and 66° < $\angle(\hat{k},\hat{B})$ < 90° contains type 1 waves with one exception $\angle(\hat{k},\hat{\phi})$ = 59°.

Fig.5. The local average magnetic field <B> vs. peak frequency (and periods, at top). The points

are coded according to analysis interval length with the same key as in the box in Figure 4. The dashed line is a least-squares fit to all points where <B> < 27 nT; the fit had a correlation coefficient of 0.498. The gyrofrequencies of O^+ and H^+ (solid lines) are shown for comparison**.**

Fig.6. Power spectral density vs. radial distance (R) from Saturn and vs. planetographic latitude (LAT), shown according to wave type, defined in the box. The point denoted by a square is neither type 1 or 2.

Fig.7.An example of Plasma Science (PLS) electron data and magnetic field differences (as in Fig. 2) for three hours of data in the mantle, showing correlations between electron density, field magnitude and field components. The top curve in the PLS panel (N_e) represents total electron density and the bottom curve represents the density of the cool electrons i.e., the so-called core component (N_C). "CODE 1" in the ΔB_θ panel shows the first analysis interval used in this study (see Table 1).

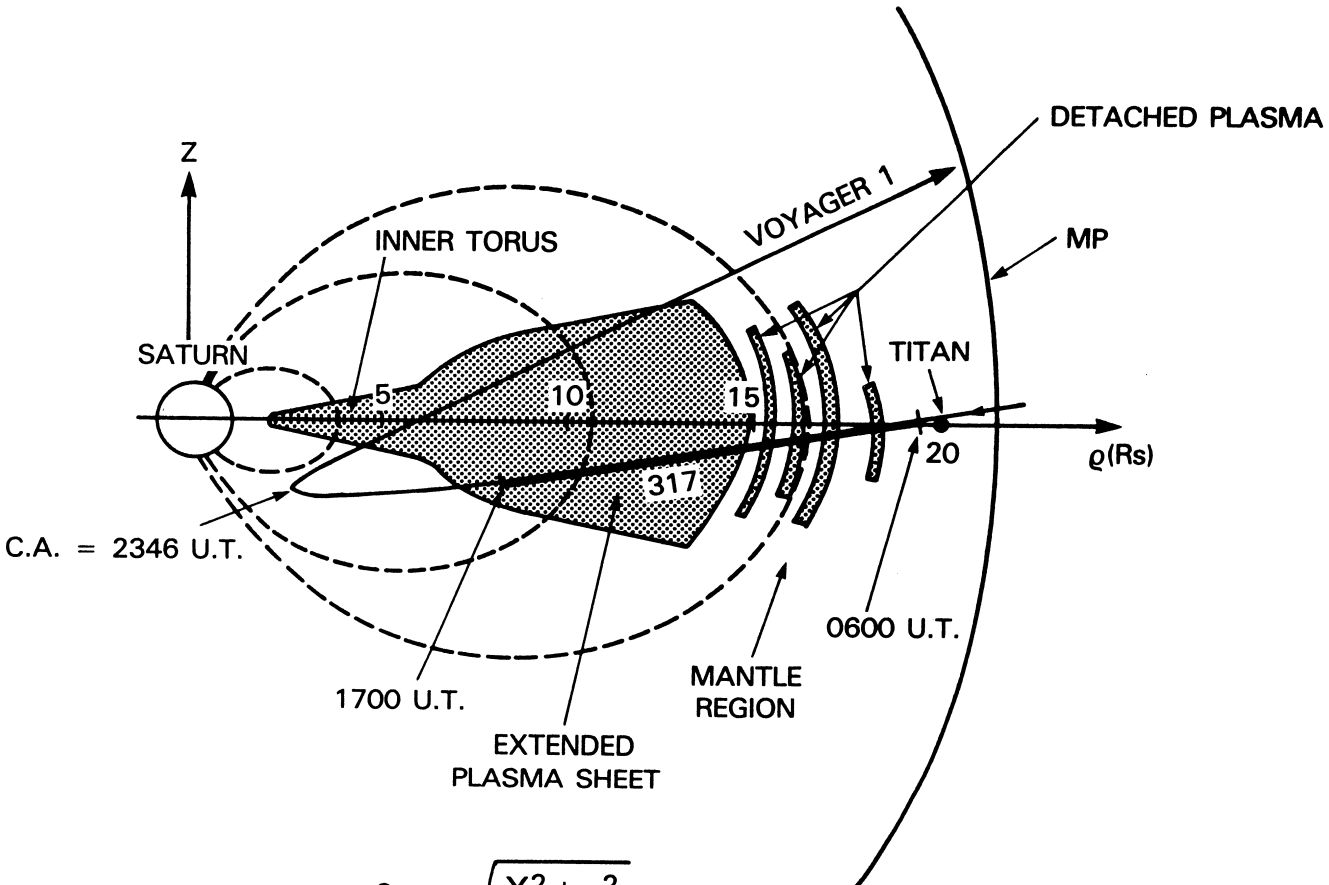

$$\varrho = \sqrt{X^2 + y^2}$$

Figure 1

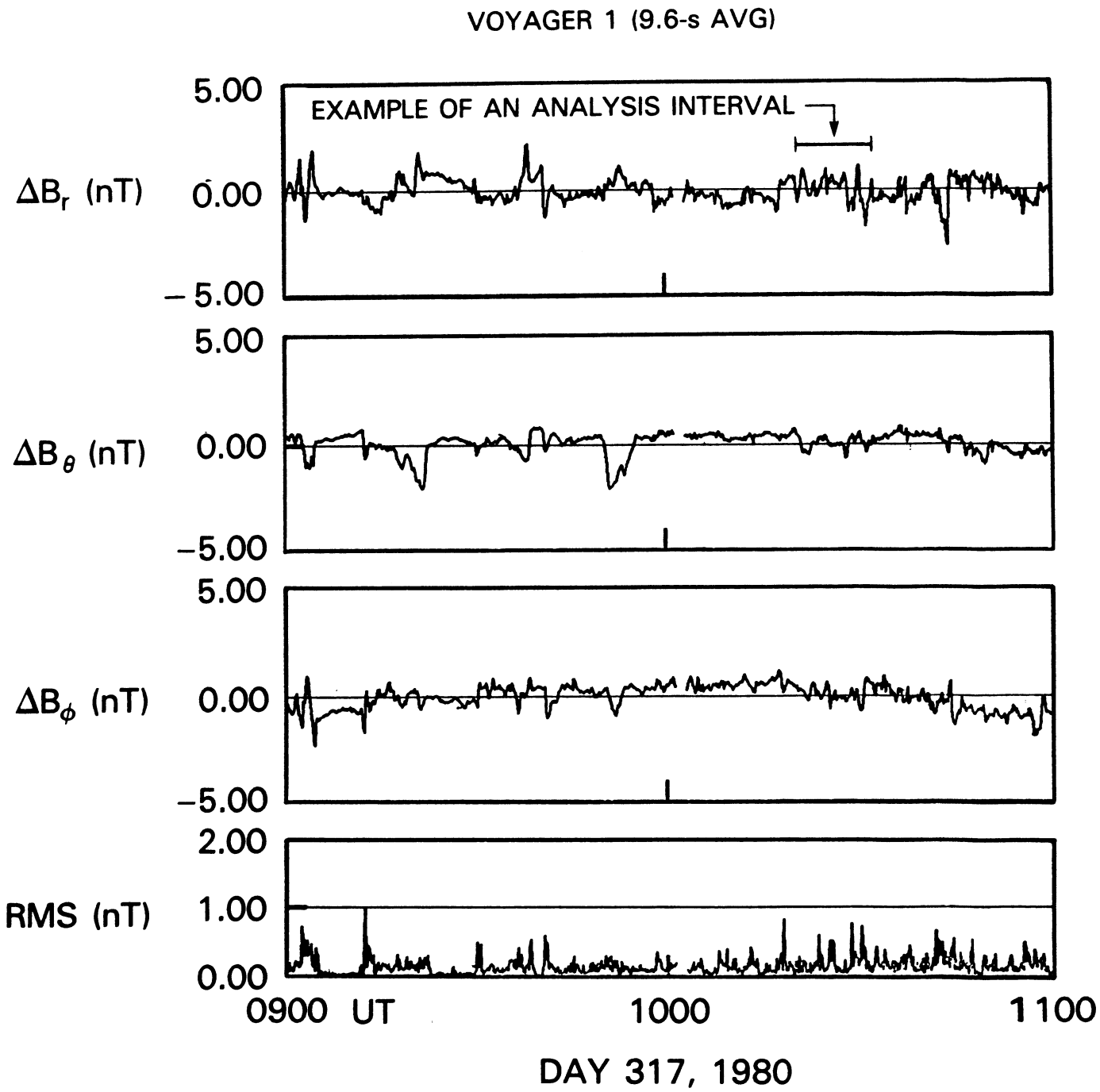
VOYAGER 1 (9.6-s AVG)
EXAMPLE OF AN ANALYSIS INTERVAL
5.00
0.00
−5.00
ΔBr (nT)
5.00
0.00
−5.00
ΔBθ (nT)
5.00
0.00
−5.00
ΔBφ (nT)
2.00
1.00
0.00
RMS (nT)
0900 UT
1000
1100
DAY 317, 1980

Figure 2

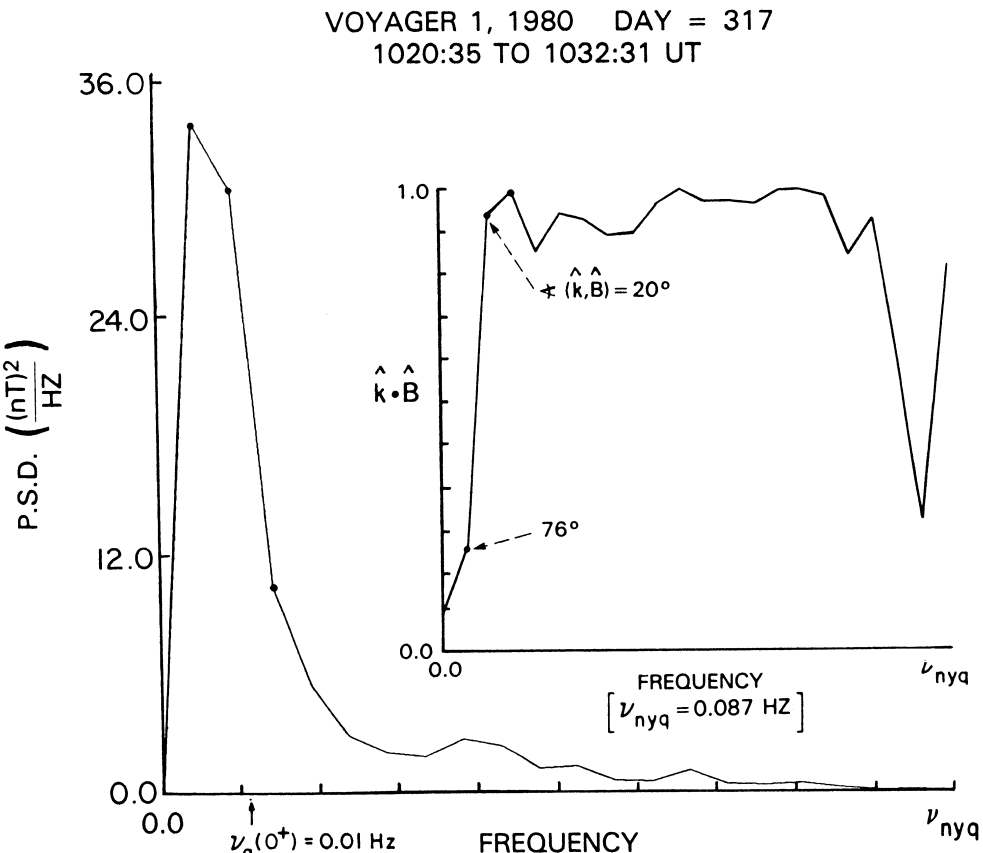
VOYAGER 1, 1980 DAY = 317
1020:35 TO 1032:31 UT
36.0
24.0
12.0
0.0
0.0
P.S.D. $\left(\frac{(nT)^2}{HZ}\right)$
$\nu_g(0^+) = 0.01$ Hz
FREQUENCY
ν_{nyq}
1.0
0.0
$\hat{k} \cdot \hat{B}$
$\angle(\hat{k},\hat{B}) = 20°$
76°
0.0
FREQUENCY
$\left[\nu_{nyq} = 0.087 \text{ HZ}\right]$
ν_{nyq}

Figure 3

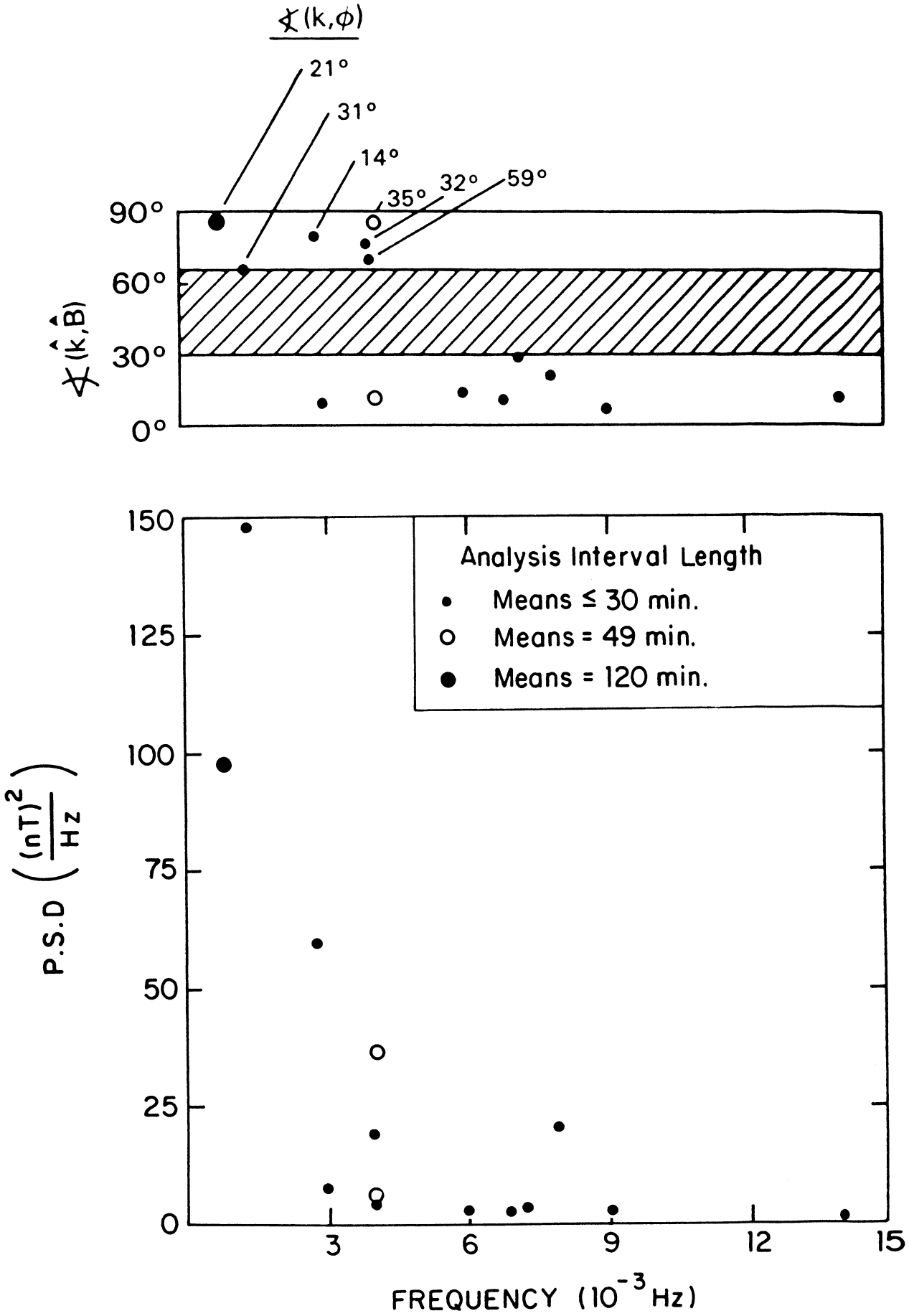
∢(k,φ)
21°
31°
14°
35°
32°
59°
90°
60°
30°
0°
∢(k̂,B̂)
150
125
100
75
50
25
0
Analysis Interval Length
Means ≤ 30 min.
Means = 49 min.
Means = 120 min.
P.S.D ((nT)²/Hz)
3
6
9
12
15
FREQUENCY (10⁻³ Hz)

Figure 4

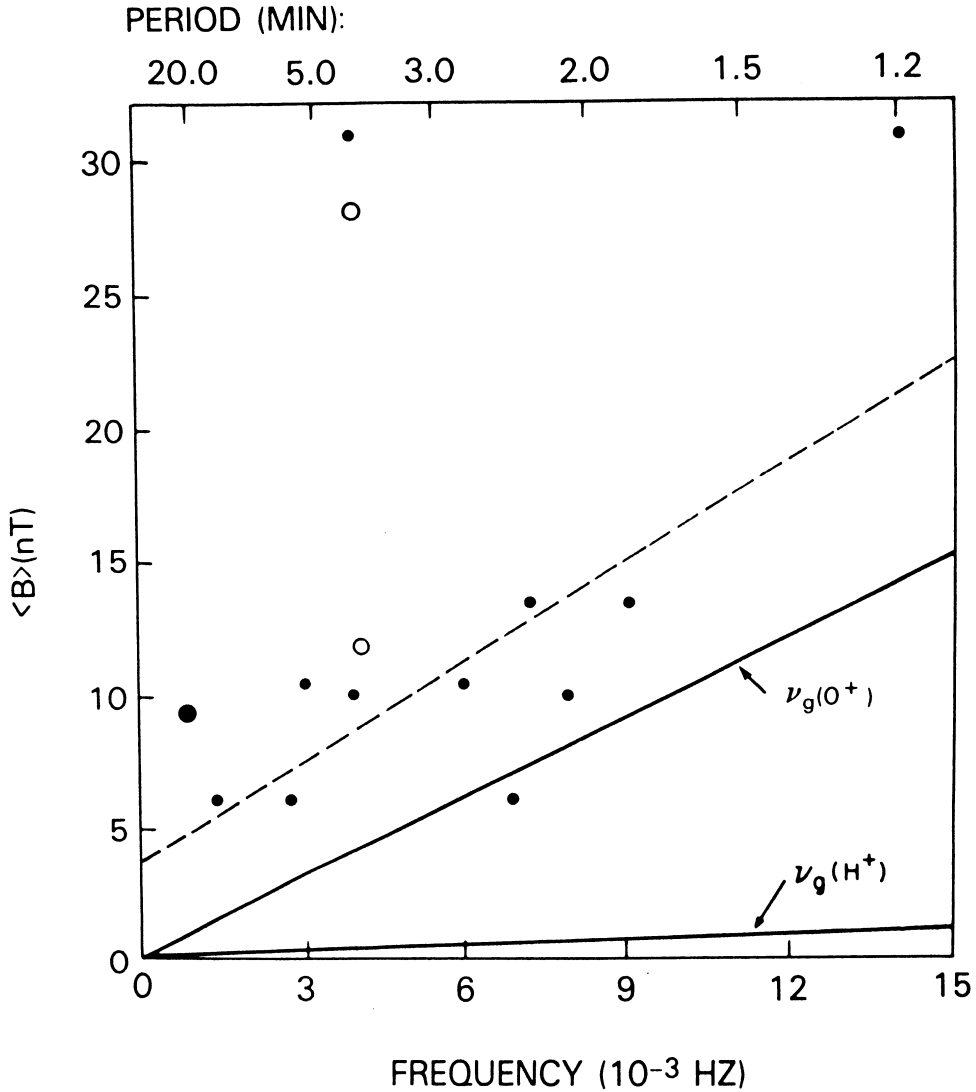
PERIOD (MIN):
20.0
5.0
3.0
2.0
1.5
1.2
30
25
20
15
10
5
0
<B>(nT)
$\nu_g(O^+)$
$\nu_g(H^+)$
0
3
6
9
12
15
FREQUENCY (10^{-3} HZ)

Figure 5

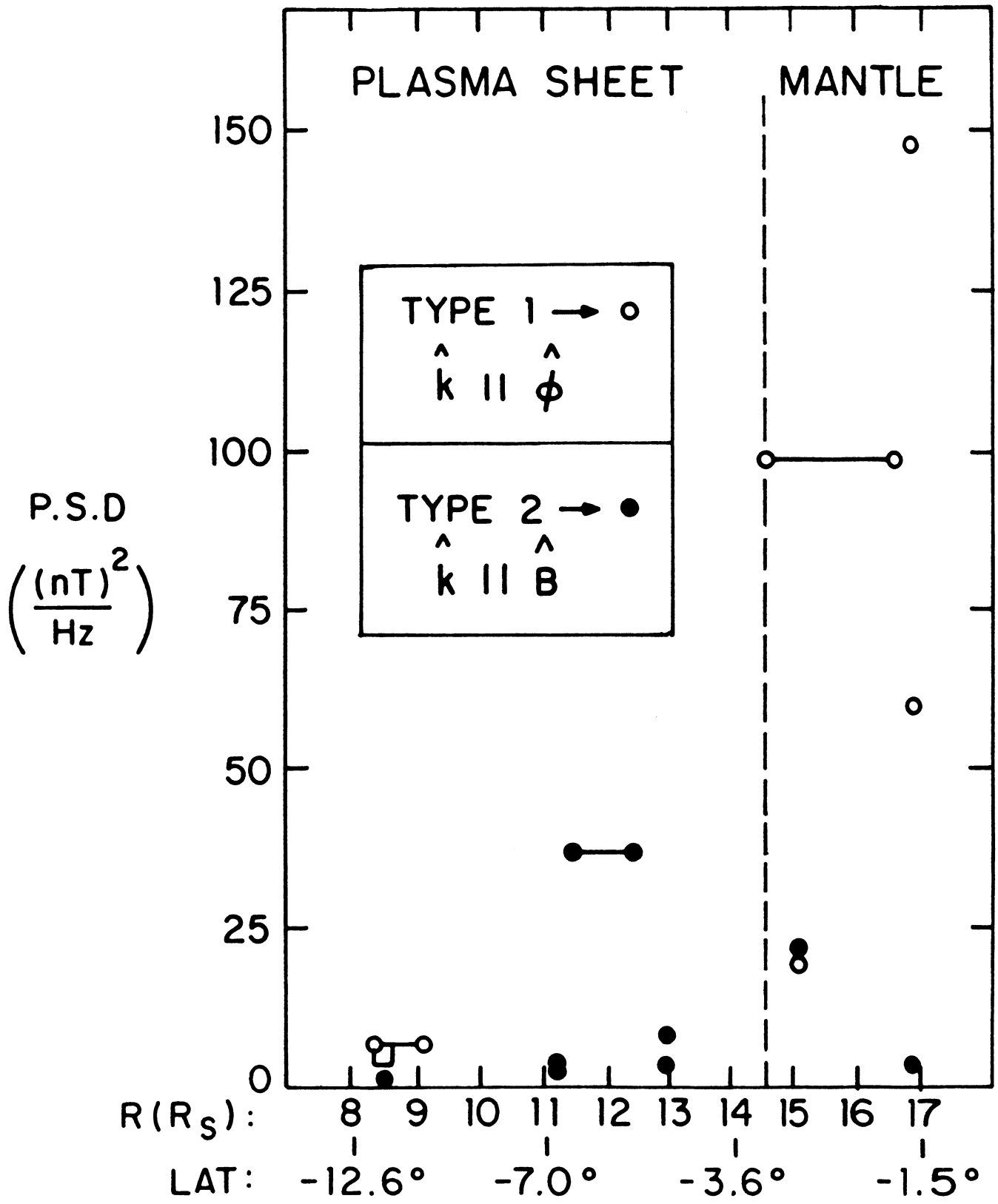
PLASMA SHEET
MANTLE
150
125
100
75
50
25
0
P.S.D
$\left(\frac{(nT)^2}{Hz}\right)$
TYPE 1 → o
$\hat{k}$ 11 $\hat{\phi}$
TYPE 2 → ●
$\hat{k}$ 11 $\hat{B}$
R(R_S): 8 9 10 11 12 13 14 15 16 17
LAT: -12.6° -7.0° -3.6° -1.5°

Figure 6

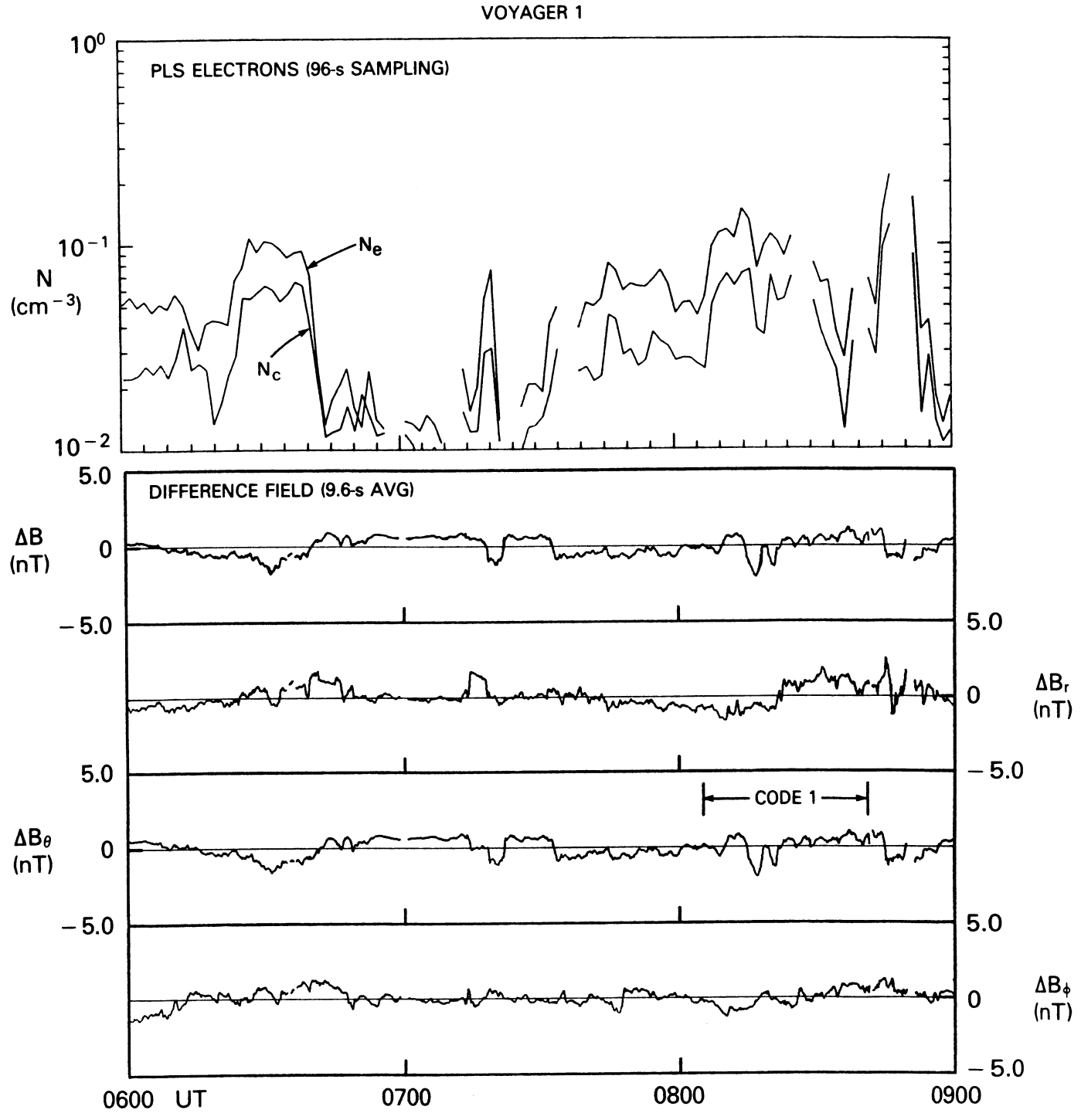
VOYAGER 1
PLS ELECTRONS (96-s SAMPLING)
10^0
10^{-1}
10^{-2}
N
(cm^{-3})
N_e
N_c
DIFFERENCE FIELD (9.6-s AVG)
ΔB
(nT)
5.0
0
−5.0
ΔB_r
(nT)
CODE 1
ΔB_θ
(nT)
ΔB_ϕ
(nT)
0600 UT
0700
0800
0900
DAY 317, 1980

Figure 7